J|A|C|S
ARTICLES
Published on Web 02/11/2003

Complex α-MoO_3 Nanostructures with External Bonding Capacity for Self-Assembly

Xiong Wen Lou and Hua Chun Zeng*

Contribution from the Department of Chemical and Environmental Engineering, Faculty of Engineering, National University of Singapore, 10 Kent Ridge Crescent, Singapore 119260

Received October 24, 2002; E-mail: chezhc@nus.edu.sg

Abstract: Through manipulating crystal growth directions, we devised a versatile synthetic method to fabricate complex α-MoO_3 nanostructures with external bonding capacity for self-organization. Using four-armed forklike α-MoO_3 as nanobuilding blocks, we assembled more complex crystal morphologies, such as centrally holed nanorods, tridents, and paintbrushes. With prolonged ultrasonic treatments, pristine forklike α-MoO_3 crystals can be turned into less armed nanostructures, giving away the secondary arms (width < 100 nm) at the same time. On the other hand, the resultant α-MoO_3 itself can act as a template to produce shaped TiO_2 and other nanocrystals. Square- and horseshoe-shaped nanocrystals of anatase TiO_2 are left undissolved after removing α-MoO_3 templates in basic medium.

Introduction

Metal oxides and sulfides stand as an important family in nanomaterials fabrication,[1−30] and they are often prepared via wet-chemical methods such as hydrothermal or solvothermal synthesis.[2,5−7] To constitute a complete toolbox for the "bottom-up" approach in nanoscience and nanotechnology,[2] the ability of making these functional materials into various artificial kits and parts is essential. In addition to the known object geometries such as dots, rods, wires, ribbons, belts, tubes, and disks,[1−30] more complex building blocks are expected to become available in the foreseeable future for device applications. From the fundamental viewpoint, furthermore, these inorganic nanoobjects should also possess external bonding capacity or "adhesiveness" for self-assembly and self-alignment in analogy to artificial supramolecular entities.[31] For example, without the assistance of organic surfactants, intrinsic joinable features or extruding arms/teeth/feelers for external connectivity might soon become a must for nanoarchitectures besides materials selection.[32] To achieve this goal, as a first step, a model synthetic scheme should be devised, ideally aiming at a total wet-chemical strategy.

Many functional materials are structurally anisotropic, which may lead to variation in growth rates along different crystallographic directions in the synthesis.[2,33] If we can switch *on* and *off* the crystal growth along a specific crystallographic direction at a particular time, in principle, crystals with complex geometric forms can be engineered.[34] Recently, we have

(1) (a) Rao, C. N. R.; Cheetham, A. K. *J. Mater. Chem.* **2001**, *11*, 2887. (b) Rao, C. N. R.; Kulkarni, G. U.; Thomas, P. J.; Edwards, P. P. *Chem.-Eur. J.* **2002**, *8*, 29.
(2) Patzke, G. R.; Krumeich, F.; Nesper, R. *Angew. Chem., Int. Ed.* **2002**, *41*, 2446.
(3) Liu, C.; Zou, B.; Rondinone, A. J.; Zhang, Z. J. *J. Am. Chem. Soc.* **2001**, *123*, 4344.
(4) Wang, J.; Rose, K. C.; Lieber, C. M. *J. Phys. Chem. B* **1999**, *103*, 8405.
(5) Penn, R. L.; Banfield, J. F. *Science* **1998**, *281*, 969.
(6) Chemseddine, A.; Moritz, T. *Eur. J. Inorg. Chem.* **1999**, 235.
(7) Pacholski, C.; Kornowski, A.; Weller, H. *Angew. Chem., Int. Ed.* **2002**, *41*, 1188.
(8) (a) Satishkumar, B. C.; Govindaraj, A.; Vogl, E. M.; Basumallick, L.; Rao, C. N. R. *J. Mater. Res.* **1997**, *12*, 604. (b) Satishkumar, B. C.; Govindaraj, A.; Nath, M.; Rao, C. N. R. *J. Mater. Chem.* **2000**, *10*, 2115.
(9) (a) Huang, M. H.; Wu, Y.; Feick, H.; Tran, N.; Weber, E.; Yang, P. *Adv. Mater.* **2001**, *13*, 113. (b) Huang, M. H.; Mao, S.; Feick, H.; Yan, H.; Wu, Y.; Kind, H.; Webber, E.; Russo, R.; Yang, P. *Science* **2001**, *292*, 1897.
(10) Niederberger, M.; Krumeich, F.; Muhr, H.-J.; Müller, M.; Nesper, R. *J. Mater. Chem.* **2001**, *11*, 1941.
(11) Zach, M. P.; Ng, K. H.; Penner, R. M. *Science* **2000**, *290*, 2120.
(12) Lou, X. W.; Zeng, H. C. *Chem. Mater.* **2002**, *14*, 4781.
(13) Pan, Z. W.; Dai, Z. R.; Ma, C.; Wang, Z. L. *J. Am. Chem. Soc.* **2002**, *124*, 1817.
(14) Wang, X.; Li, Y. *J. Am. Chem. Soc.* **2002**, *124*, 2880.
(15) Pan, Z. W.; Dai, Z. R.; Wang, Z. L. *Science* **2001**, *291*, 1947.
(16) Iijima, S. *Nature* **1991**, *354*, 56.
(17) Tenne, R.; Margulis, L.; Genut, M.; Hodes, G. *Nature* **1992**, *360*, 444.
(18) Feldman, Y.; Wasserman, E.; Srolovitz, D. J.; Tenne, R. *Science* **1995**, *267*, 222.
(19) Chhowalla, M.; Amaratunga, G. A. J. *Nature* **2000**, *407*, 164.
(20) Hsu, W. K.; Zhu, Y. Q.; Boothroyd, C. B.; Kinloch, I.; Trasobares, S.; Terrones, H.; Grobert, N.; Terrones, M.; Escudero, R.; Chen, G. Z.; Colliex, C.; Windle, A. H.; Fray, D. J.; Kroto, H. W.; Walton, D. R. M. *Chem. Mater.* **2000**, *12*, 3541.
(21) Remskar, M.; Mrzel, A.; Skraba, Z.; Jesih, A.; Ceh, M.; Demsar, J.; Stadelmann, P.; Levy, F.; Mihailovic, D. *Science* **2001**, *292*, 479.
(22) Brorson, M.; Hansen, T. W.; Jacobsen, C. J. H. *J. Am. Chem. Soc.* **2002**, *124*, 11582.
(23) Sone, E. D.; Zubarev, E. R.; Stupp, S. I. *Angew. Chem., Int. Ed.* **2002**, *41*, 1706.
(24) Ajayan, P. M.; Stephan, O.; Redlich, P.; Colliex, C. *Nature* **1995**, *375*, 564.
(25) Spahr, M. E.; Bitterli, P.; Nesper, R.; Müller, M.; Krumeich, F.; Nissen, H.-U. *Angew. Chem., Int. Ed.* **1998**, *110*, 1339.
(26) Nakamura, H.; Matsui, Y. *J. Am. Chem. Soc.* **1995**, *117*, 2651.
(27) (a) Martin, C. R. *Science* **1994**, *266*, 1961. (b) Lakshmi, B. B.; Dorhout, P. K.; Martin, C. R. *Chem. Mater.* **1997**, *9*, 857. (c) Lakshmi, B. B.; Patrissi, C. J.; Martin, C. R. *Chem. Mater.* **1997**, *9*, 2544.
(28) (a) Kobayashi, S.; Hanabusa, K.; Hamasaki, N.; Kimura, M.; Shirai, H.; Shinkai, S. *Chem. Mater.* **2000**, *12*, 1523. (b) Jung, J. H.; Kobayashi, H.; van Bommel, K. J. C.; Shinkai, S.; Shimizu, T. *Chem. Mater.* **2002**, *14*, 1445. (c) Kobayashi, S.; Hamasaki, N.; Suzuki, M.; Kimura, M.; Shirai, H.; Hanabusa, K. *J. Am. Chem. Soc.* **2002**, *124*, 6550.
(29) Vayssieres, L.; Keis, K.; Hagfeldt, A.; Lindquist, S.-E. *Chem. Mater.* **2001**, *13*, 4395.
(30) Dai, Z. R.; Pan, Z. W.; Wang, Z. L. *J. Am. Chem. Soc.* **2002**, *124*, 8673.
(31) Lehn, J.-M. *Science* **2002**, *295*, 2400.
(32) Sampanthar, J. T.; Zeng, H. C. *J. Am. Chem. Soc.* **2002**, *124*, 6668.
(33) (a) Zeng, H. C. *Inorg. Chem.* **1998**, *37*, 1967. (b) Zeng, H. C.; Sheu, C. W.; Hia, H. C. *Chem. Mater.* **1998**, *10*, 974.
(34) (a) Zeng, H. C.; Chong, T. C.; Lim, L. C.; Kumagai, H.; Hirano, M. *J. Cryst. Growth* **1996**, *160*, 289. (b) Zeng, H. C.; Chong, T. C.; Lim, L. C.; Kumagai, H.; Hirano, M. *J. Cryst. Growth* **1996**, *160*, 296. (c) Zeng, H. C. *J. Cryst. Growth* **1997**, *173*, 446.

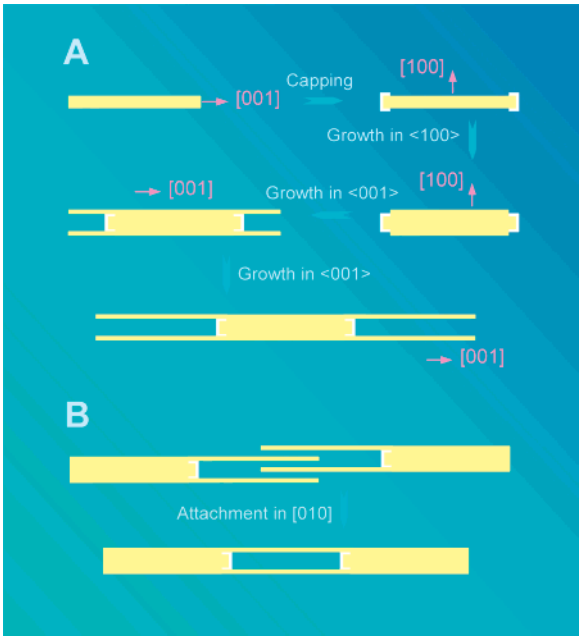

Figure 1. (A) Flowchart of synthesis of forklike α-MoO_3 nanostructures (in light yellow) via manipulating growth directions; TiO_2 capping (in white) is also indicated. (B) Oriented attachment between two forklike nanostructures along the [010] direction (perpendicular to the paper).

developed a hydrothermal method to grow one-dimensional (1D) α-MoO_3 and 2H-MoS_2 nanorods with a subsequent sulfidation.[12] On the basis of these results, in this article, we will demonstrate a novel synthetic scheme to manipulate the growth directions of α-MoO_3 under hydrothermal conditions. This method, together with oriented self-assembly of the resultant nanounits, allows us to generate geometrically complex α-MoO_3 nanostructures with external bonding capacity (e.g., armed and/or holed forklike rods, tridents, and paintbrushes). The method is highly versatile, because it also allows us to utilize the grown α-MoO_3 as templates for making other complex nanomaterials such as anatase TiO_2 in the present study.

Experimental Section

Materials Preparation. The hydrothermal experiments for the synthesis of 1D α-MoO_3 nanostructures had been described in detail in our previous publication.[12] This process involves an acidification of ammonium heptamolybdate tetrahydrate (AHM; $(NH_4)_6Mo_7O_{24}\cdot 4H_2O$) in nitric acid to form an intermediate compound $((NH_4)_2O)_{0.0866}\cdot MoO_3\cdot 0.231H_2O$ and a subsequent conversion of this solid phase to final α-MoO_3 under the acidic condition. In the present work, the preparation of complex α-MoO_3 nanostructures can be broadly described as a three-stage process (Figure 1A): (i) synthesis of 1D α-MoO_3 from intermediate crystal $((NH_4)_2O)_{0.0866}\cdot MoO_3\cdot 0.231H_2O$, (ii) capping the 1D α-$MoO_3$ with TiO_2, and (iii) directional growth of α-MoO_3 on the TiO_2-capped nanostructure. It is further proved that stages (i) and (ii) can be combined, which maximizes the end capping population of the TiO_2/α-MoO_3 nanorods. A typical combined synthesis is summarized here: 5.0 mL of an AHM solution (saturated at room temperature, aged for more than 1 month) was mixed with 10.0 mL of 2.2 M nitric acid, followed by hydrothermal treatment at 170 °C for 20 h in a Teflon-lined stainless steel autoclave. As-prepared solid product at this stage was $((NH_4)_2O)_{0.0866}\cdot MoO_3\cdot 0.231H_2O$. Later, 5.0 mL of TiF_4 (0.04 M) was added to this suspension (containing the intermediate crystallites $((NH_4)_2O)_{0.0866}\cdot MoO_3\cdot 0.231H_2O$). The mixture was heated under hydrothermal condition at 170 °C for 24−30 h. Depending on the fine turning of the synthetic parameters and the amount of TiF_4 added, the TiO_2 (in anatase phase) could be deposited only to both ends of the α-MoO_3 nanorods or to an entire surface of the rods. In stage (iii) synthesis, 0.05−0.08 g of the intermediate crystal compound $((NH_4)_2O)_{0.0866}\cdot MoO_3\cdot 0.231H_2O$ (obtained from a separate synthesis) and 15.0 mL of 2.2 M nitric acid were added to about 0.03 g of TiO_2-capped α-MoO_3 nanorods prepared from stages (i) and (ii). Thereafter, the suspension mixture was hydrothermally treated at 200 °C for around 10 h, which produced complex α-MoO_3 nanostructures because of the controlled directional growths. The solid products were then separated from the solution via filtration, followed by a thorough washing with deionized water and drying at around 60 °C in an electric oven.

Materials Characterization. Crystallographic information of α-MoO_3 nanostructures including the deposited TiO_2 was investigated with powder X-ray diffraction (XRD; Shimadzu XRD-6000, Cu Kα, λ = 1.5406 Å). Chemical compositions of anatase TiO_2 and α-MoO_3 crystals were investigated with X-ray photoelectron spectroscopy (XPS; AXIS-Hsi, Kratos Analytical) using a monochromatized Al Kα exciting radiation ($h\nu$ = 1486.71 eV). XPS spectra of Mo 3d, Ti 2p, and O 1s were measured with a constant analyzer-pass energy of 40.0 eV. All binding energies (BE) were referenced to the C 1s peak (BE = 284.7 eV) arising from adventitious carbon. Prior to the peak deconvolution, X-ray satellites and inelastic background (Shirley-type) were subtracted for all spectra, as done in our previous XPS investigations. High-resolution analytical transmission electron microscopy (HRTEM, Philips FEG CM300, 300 kV, with EDX; and TEM, JEM-2010, 200 kV) and selected area electron diffraction (SAED) were used to examine the crystal products. Elemental composition of individual α-MoO_3 nanostructures was also confirmed with energy dispersive spectroscopy (EDX) microanalysis. The specimens for HRTEM/TEM/SAED/EDX studies were prepared by suspending solid samples in acetone with ultrasonic dispersion (0.5−5 h in a water bath; mostly 0.5−0.75 h); the details are similar to those of our previous work.[12,32]

Results and Discussion

Figure 1A depicts the controlled synthesis of complex α-MoO_3 nanounits in this work. For naturally grown α-MoO_3 crystals and nanocrystals, a rectangular morphology is observed (the first yellow bar, Figure 1A): [001] ≫ [100] ≫ [010] because of the intrinsic structural anisotropy and growth rate (r_{hkl}) variation in all three principal directions $r_{001} \gg r_{100} \gg r_{010}$.[33] With the capping of TiO_2 in the two ⟨001⟩ ends (white "nail heads", Figure 1A), the growth of α-MoO_3 nanorods in ⟨001⟩ is switched off (due to a high energy barrier of heterogeneous nucleation, i.e., MoO_3 on TiO_2), and their further growth is forced to the ⟨100⟩ direction (this growth requires only homogeneous nucleation, i.e., MoO_3 on MoO_3). When the crystal along [100] exceeds the dimension of TiO_2 caps (i.e., rims of the nail heads), the faster growth along ⟨001⟩ of α-MoO_3 will resume, noting that the growth rate of ⟨001⟩ is much greater than that of ⟨100⟩.[33] This staged manipulation will result in different α-MoO_3 nanocrystals with complex geometrical structures, as is shown with four secondary α-MoO_3 rods along ⟨001⟩, which gives rise to an overall double-ended forklike morphology (the final product, Figure 1A).

Figure 2A displays our TiO_2-capped α-MoO_3 nanorods synthesized from stages (i) and (ii). As shown here, by introducing a correct amount of TiF_4 in the synthesis, the TiO_2 crystallites can attach exclusively to the growing ends ({001} surfaces) of α-MoO_3 nanorods, while no deposition on the surfaces of {100} and {010} is found. This is further illustrated in Figure 2B where an extra amount of TiF_4 was added to the synthesis. Instead of the nail-like structure (Figure 2A), much larger crystals of TiO_2 including those at both ends are formed

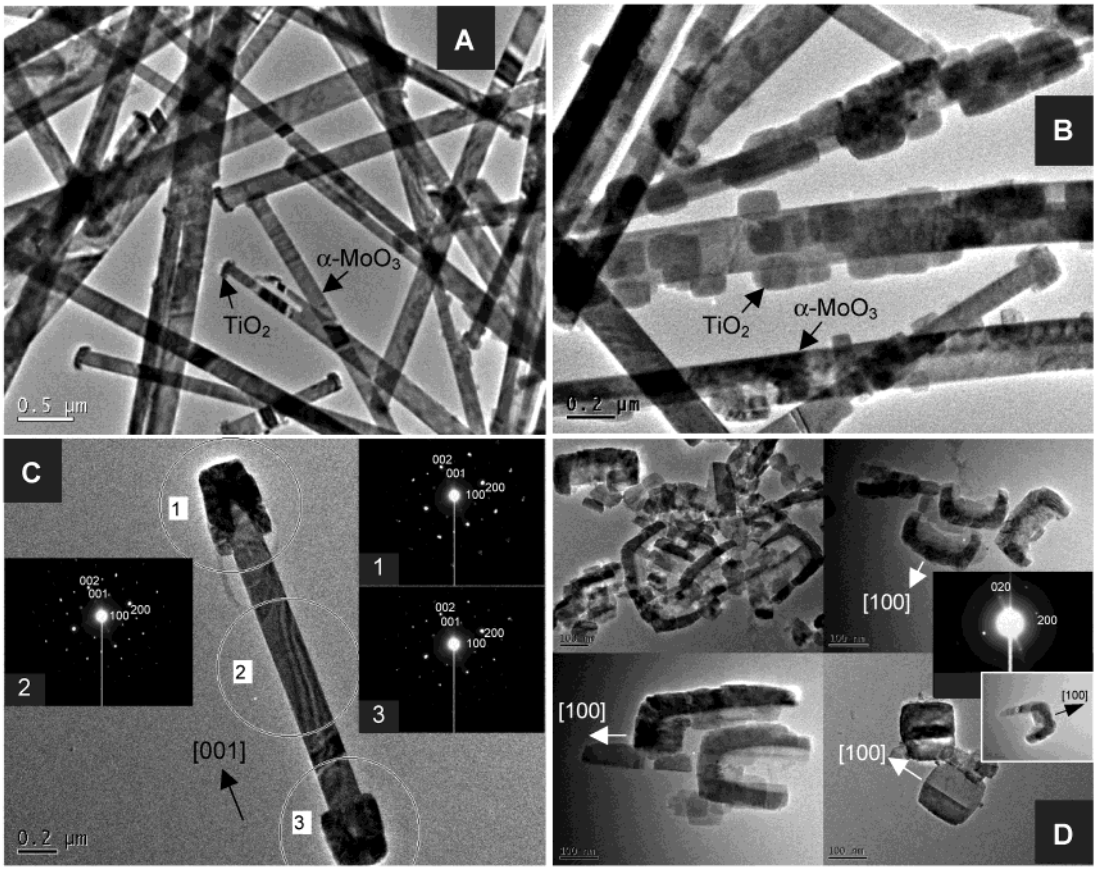

Figure 2. (A) TiO_2-capped α-MoO_3 nanorods synthesized from a combined synthesis at 170 °C (20 + 24 h, see Experimental Section). (B) Sample prepared in a way similar to (A) but with an additional 3 mL of TiF_4 in a third heating of 10 h (i.e., 21 + 30 + 10 h). (C) SAED patterns ([010] zone of α-MoO_3) of a thick TiO_2-capped α-MoO_3 nanorod prepared with 0.0328 g of thin TiO_2-capped α-MoO_3 nanorods (similar to (A)), 0.0830 g of $((NH_4)_2O)_{0.0866}$·MoO_3·$0.231H_2O$, 5 mL of TiF_4, and 15 mL of HNO_3 solution at 170 °C for 32 h. (D) TiO_2 nanocrystals after removing α-MoO_3 templates (i.e., sample of (B) dissolved with ammonia solution). The ED pattern ([001] zone of anatase TiO_2) belongs to a horseshoe-shaped TiO_2 crystal (white inset). All scale bars in (D) are 100 nm.

on the surfaces of α-MoO_3 nanorods (Figure 2B). The crystallographic phase of the deposited TiO_2 is in anatase polymorph (confirmed by XRD, tetragonal symmetry, $a = 3.7852$ Å and $c = 9.5139$ Å).[35,36] The α-MoO_3 substrate has an orthorhombic symmetry with lattice constants of $a = 3.9630$ Å, $b = 13.856$ Å, and $c = 3.6966$ Å.[37,38] The selection of anatase TiO_2 for the cessation of the α-MoO_3 [001] growth is based on the close resemblance of the lattice parameters. Lattice mismatches between the {001} planes of anatase TiO_2 and the {010} planes of α-MoO_3 are only −4.5 and 2.4%, respectively, along [100] and [001] of α-MoO_3. A close examination of Figure 2B indicates that the crystals are indeed squarelike and arranged orderly according to the crystallographic orientations of α-MoO_3. The growth of anatase TiO_2 on α-MoO_3 is apparently epitaxial. This is further confirmed with our SAED results shown in Figure 2C for a dumbbell-like TiO_2-capped α-MoO_3 nanorod. The wavy image contrasts observed in this rod are due to a slight bending strain (the MoO_3 rod wears two TiO_2 "horseshoes"!). In general, the three SAED patterns are very similar, indicating an excellent lattice matching between the two different materials. The pattern for the α-MoO_3 part (2, middle of the rod) can be assigned to *h*0*l* diffraction spots ([010] zone) according to the extinction rule for space group *Pbnm*. On the other hand, in view of small variations of lattice parameters, the same set of spots can also be attributed to the *hk*0 diffraction spots ([001] zone) of the aligned TiO_2 crystals (two ends of the rod), noting that the space group of anatase TiO_2 ($I4_1/amd$) allows only even *h* and *k* spots to be shown. Therefore, the patterns (1 and 3) from the two ends of the rod can be attributed to a superimposition of the above two sets of diffraction spots, which is further evidenced in a slight divergence of spots observed for the higher order beams. Furthermore, the deposited TiO_2 can be separated from α-MoO_3 nanorods. As shown in Figure 2D, α-MoO_3 nanorods can be dissolved completely in ammonia solution, leaving only TiO_2 nanocrystals. It is revealed that the horseshoe-shaped TiO_2 (from the end capping) comprises small but well-arranged crystals, while the squarelike TiO_2 (viewed along [001]) is largely single-crystalline. The orientations of TiO_2 are further confirmed with SAED experiments (inset, Figure 2D) and the as-grown crystal facets {100} and {010}, noting that the relations between the squared TiO_2 crystals and α-MoO_3 substrate are registered in the growth marks when the template was removed (see the lower right of Figure 2D). All of the above experiments indicate that the *a*-axes of TiO_2 crystals are parallel

(35) Joint Committee on Powder Diffraction Standards, International Centre for Diffraction Data, Card No. 21-1272, Swarthmore, PA, 1996.
(36) Herman, G. S.; Gao, Y. *Thin Solid Films* **2001**, *397*, 157.
(37) Joint Committee on Powder Diffraction Standards, International Centre for Diffraction Data, Card No. 35-0609, Swarthmore, PA, 1996.
(38) (a) Hsu, Z. Y.; Zeng, H. C. *J. Phys. Chem. B* **2000**, *104*, 11891. (b) Zeng, H. C.; Ng, W. K.; Cheong, L. H.; Xie, F.; Xu, R. *J. Phys. Chem. B* **2001**, *105*, 7178. (c) Zeng, H. C.; Xie, F.; Wong, K. C.; Mitchell, K. A. R. *Chem. Mater.* **2002**, *14*, 1788.

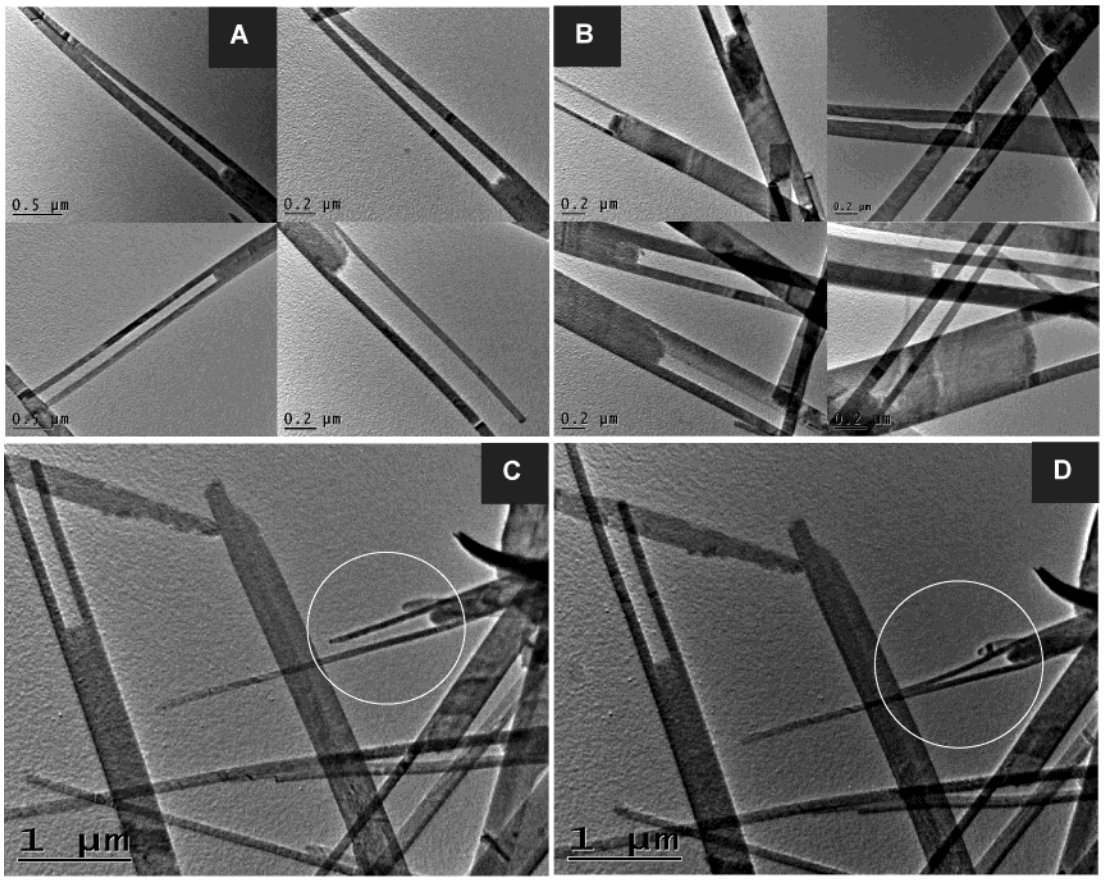

Figure 3. Forklike α-MoO_3 nanorods prepared with 0.030 g of TiO_2-capped α-MoO_3, 0.0841 g of $((NH_4)_2O)_{0.0866}{\cdot}MoO_3{\cdot}0.231H_2O$, and 15 mL of HNO_3 solution at 200 °C for 10.5 h: (A and B) free-standing rods, and (C and D) arm-clamping process during the TEM measurement.

to the *a*- and *c*-axes of α-MoO_3, respectively, while the *c*-axis is parallel to the *b*-axis of their substrate.

With the capping of TiO_2 in the ⟨001⟩ direction (nail heads, Figures 1A and 2A), the α-MoO_3 nanorods in their further growth have to change to the ⟨100⟩ direction until they exceed the dimension of the deposited TiO_2 (i.e., rims of the nail heads). The overall dimension in [100] now is greater than that of original α-MoO_3 rods because of the ⟨100⟩ growth, and the subsequent growth along ⟨001⟩ gives rise to four-armed forklike α-MoO_3 nanostructures. Depending on growth parameters (e.g., the size of TiO_2 capping in stages (i) and (ii), and growth time along ⟨100⟩ then ⟨001⟩ in stage (iii)), the observed forklike morphology takes a population ranging from 20 to 90%. Because of the excellent control of TiO_2 cap size, the growths along ⟨001⟩ are resumed approximately at the same time, which is reflected in the similar lengths of four secondary α-MoO_3 nanorods (Figure 3). The junction parts are further detailed in Figure 4. In general, the width of secondary arms is constant, indicating that the growth after stages (i) and (ii) is ⟨001⟩ predominant. This is also evidenced in the [100] dimensional values w_1 and w_2 (marked in Figure 4D), whose difference is very small for most rods. In all cases, the growth on TiO_2 capping is prohibited, as it has to encounter heterogeneous nucleation whose activation energy is apparently higher than that on the α-MoO_3. One of the important observations is the flexibility of the secondary rods. The dark lined contrasts perpendicular to [001] direction were movable during the TEM measurement, revealing that there exist certain bending strains arising from physical contacts with the carbon grid or neighboring crystallites. It has been well known that α-MoO_3 is not very stable under the energetic beam of TEM,[39] and surface charges may be induced during the measurement (Figure 3A). As demonstrated in Figure 3C and D, a pair of these secondary rods are coupling because of the electron-induced charging. In this sense, the clamping motion observed can be utilized in switching/sensing operations.

The crystal structure of this complex nanostructure is further examined in Figure 5. The SAED patterns at various locations along a forklike α-MoO_3 nanorod are identical, indicating its excellent crystalline continuity and physical integrity (i.e., a single-crystalline nanostructure). In particular, HRTEM images of the main stems and the secondary rods indicate high perfection of crystal lattices. As shown in Figure 6, lattice fringes of d_{100} (4.0 ± 0.2 Å, not shown), d_{001} (3.7 ± 0.2 Å), and d_{101} (2.7 ± 0.2 Å) can be clearly observed along the [010] direction. Note that the short distances of crystalline structure recorded are due to the high sensitivity of the α-MoO_3 sample under HRTEM measuring conditions.[39] Furthermore, EDX investigation reveals that there is no Ti element within the stems and secondary arms of α-MoO_3 nanorods (Figure 6). The oxidation states of TiO_2 capping and α-MoO_3 nanorods are further investigated in our XPS study (Figure 7). Indeed, the Mo is strictly in its highest oxidation state of +6, as evidenced in the doublet of Mo $3d_{5/2}$ (BE = 232.8 eV) and Mo $3d_{3/2}$ (BE =

(39) Dleporte, P.; Meunier, F.; Pham-Huu, C.; Vennegues, P.; Ledoux, M. J.; Guille, J. *Catal. Today* **1995**, *23*, 251.

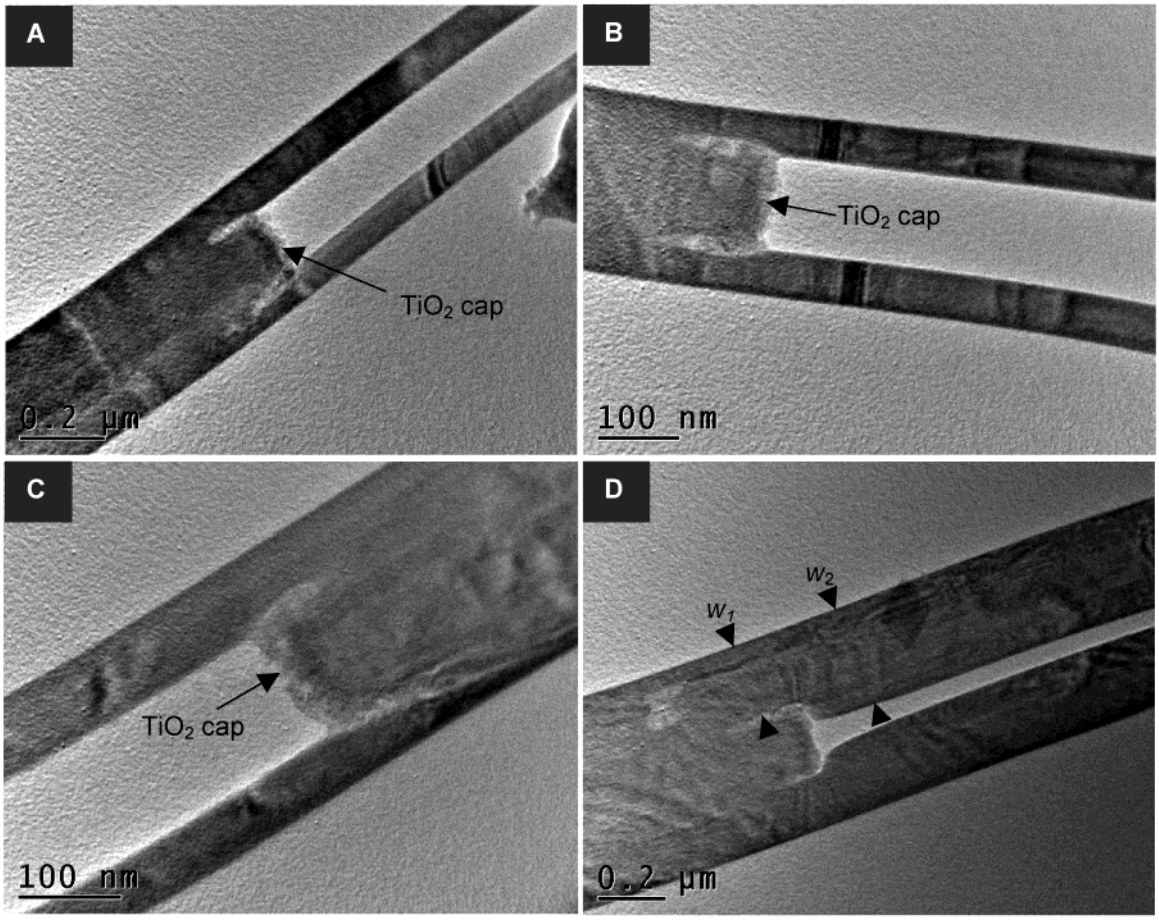

Figure 4. TEM examinations on the juncture details between TiO_2 caps and forklike α-MoO3 nanorods (A, B, C), and definition of W_1 and W_2 (D); the sample is from the same synthesis as in Figure 3.

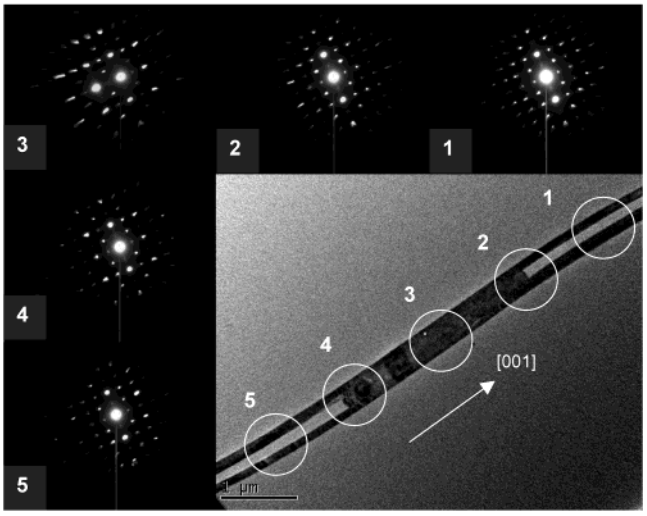

Figure 5. SAED patterns ([010] zone) along a four-armed α-MoO_3 nanorod (sample from Figure 3). Note that the electron beam is injected perpendicular to the (010) plane.

236.0 eV) for α-MoO_3 phase.[38,40] On the other hand, the oxidation state of the Ti element in this nanostructure (Ti $2p_{3/2}$, BE = 458.8 eV, and Ti $2p_{1/2}$, BE = 464.3 eV) is also identical to that of TiO_2 in the literature,[36] although its content is small. The large peak in O 1s is assigned to lattice oxygen atoms of both MoO_3 and TiO_2, while the small one is assigned to the surface hydrated oxygen.[41] These results elucidate that the atomic incorporation or substitution of Ti in α-MoO_3 crystal lattice can be ruled out, because once this occurs the formation of $Ti^{IV}-O-Mo^{VI}$ connectivity will cause a charge transfer between the two metal elements and result in significant alterations in BEs. The lack of interdiffusion between the two phases is expected because of their vast difference in oxidation states (VI vs IV). This point has been evidenced in a recent study of $TiO_2-(MoO_3)_x$ core−shell structures where no interdiffusion is observed.[42]

α-MoO_3 is a layered material in which two-dimensional MoO_3 "molecular" sheets are stacked along ⟨010⟩ by van der Waals interactions.[38] Therefore, the {010} surfaces possess a strong tendency for external bonding. The most distinguished feature of the forklike α-MoO_3 nanostructure is its four extending arms. These flexible "tentacles" (each arm has two large {010} surfaces) are able to generate intercrystallite connectivity. With the present synthetic method, the resultant forklike structures can further self-align into even more complex nanostructures. As illustrated in a model in Figure 1B, two (or more) forklike α-MoO_3 nanounits can be combined in an inward manner through their secondary arms, creating a new type of

(40) (a) Anwar, M.; Hogarth, C. A.; Bulpett, R. *J. Mater. Sci.* **1989**, *24*, 3087. (b) Spevack, P. A.; McIntyre, N. S. *J. Phys. Chem.* **1992**, *96*, 9029.

(41) Chambers, S. A.; Droubay, T.; Jennison, D. R.; Mattsson, T. R. *Science* **2002**, *297*, 827.

(42) Elder, S. H.; Cot, F. M.; Su, Y.; Heald, S. M.; Tyryshkin, A. M.; Bowman, M. K.; Gao, Y.; Joly, A. G.; Balmer, M. L.; Kolwaite, A. C.; Magrini, K. A.; Blake, D. M. *J. Am. Chem. Soc.* **2000**, *122*, 5138.

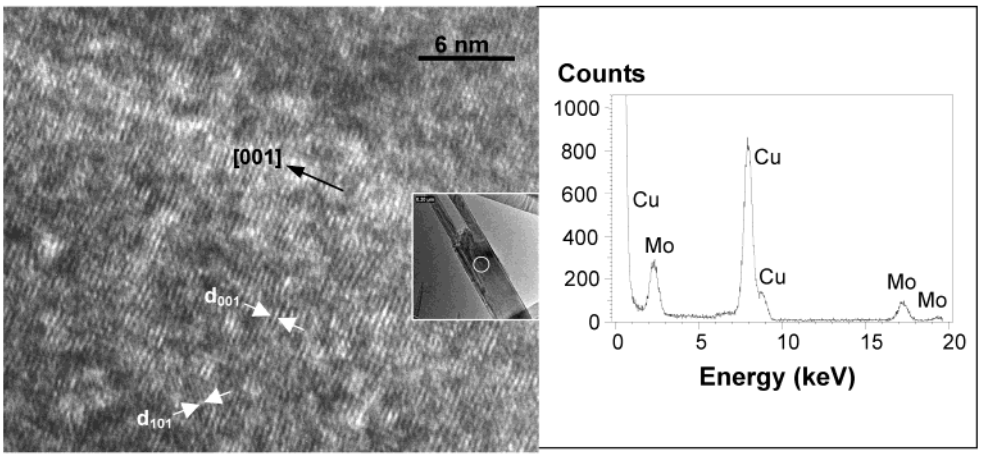

Figure 6. Lattice fringes and EDX microanalysis of a free-standing α-MoO_3 nanorod (from Figure 3); the signal of Cu is generated from the Cu grid. The inset indicates the examined location.

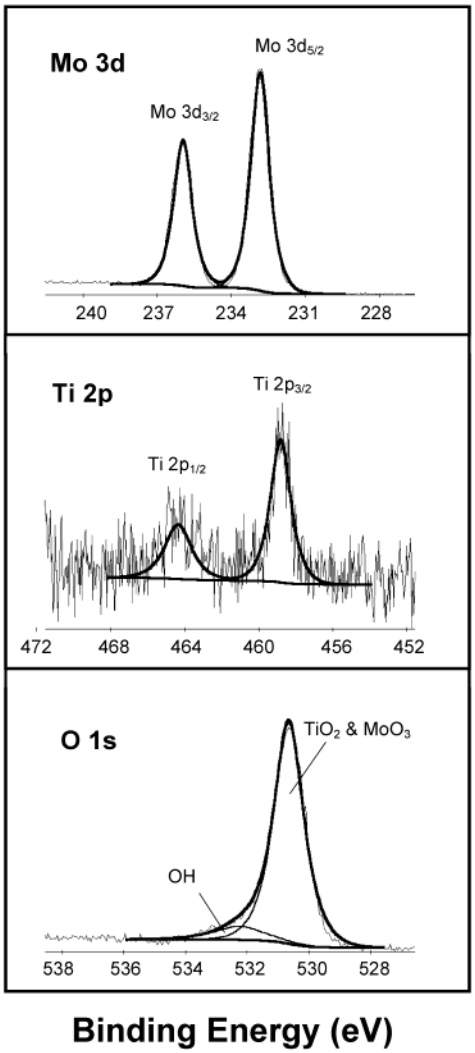

Figure 7. XPS spectra of Mo 3d, Ti 2p, and O 1s core electrons for the forklike sample from Figure 3. Peak area ratio of $Mo3d_{5/2}/Mo3d_{3/2} = 1.5$, $\Delta Mo3d = 3.1 \pm 0.1$ eV, peak area ratio of $Ti2p_{3/2}/Ti2p_{1/2} = 2.0$, and $\Delta Ti2p = 5.5 \pm 0.1$ eV.

artificial morphology. This crystal architecture is indeed realized for the first time in our synthesis, as reported in Figure 8A and B. Importantly, with the central space created, these crystals show joinable capacity for further assemblies with other nanostructures (including heteronanostructures), especially for creating an external connectivity perpendicular to the {010} planes. The perfect rectangular hole structure is evidence of a "cementing mechanism" (a larger crystal is formed from smaller ones)[43] operating in this post-growth organization. First, the forklike crystals must have similar arm spans to initiate an arm-to-arm overlapping. Second, the {010} surfaces of the crystal arms must be sufficiently smooth. Finally, as mentioned before, the arms must be flexible enough to adjust to a correct stacking order in accordance with the orthorhombic structure of α-MoO_3. In addition to the "L + R" (i.e., one from left and one from right) stacking, more than two pieces of crystals involved are possible. In Figure 8B, three forklike crystals are stacked in a "2L + 1R" (i.e., two from left and one from right) fashion using their {010} planes, generating also an empty rectangular hole. As detailed in the inset, the α-MoO_3 arms from the right-hand side crystal (3) extend over the TiO_2 capping of the crystals (1 and 2) of the left. In a similar way, "2R" or "2L" stacking has also been observed in the present work. For example, two forklike crystals use only one arm each to form a nano-trident (Figure 8C), while they can also use both of their arms to form a nano-paintbrush (Figure 8D). In all cases, overlapping between the secondary arms and main crystal stems is also possible, which is elucidated in the observed multiple TiO_2-MoO_3 junctures in the final complex nanostructures. The "cementing mechanism" has been recently explored further in the synthesis of nanostructured materials (also called "oriented attachment").[5−7] Well-investigated examples in nanometer regime are the ionic crystals of TiO_2 and ZnO,[5−7] and layered compound β-$Co(OH)_2$.[32] To the best of our knowledge, the current investigation serves as a first example of complex nanomaterial architectures with an underlying cementing mechanism operative. It should be mentioned that a considerable amount of the above "fused" types of α-MoO_3 nanostructures can be easily located in our TEM examinations, although the majority are individual nano-forks. Even without the ultrasonic treatments for our TEM suspensions (e.g., the as-synthesized solid samples were dispersed with only mechanical stirring in deionized water), the same complex α-MoO_3 nanostructures (all of the above types) can still be observed, which indicates that the observed

(43) (a) Kolthoff, I. M.; Noponen, G. E. *J. Am. Chem. Soc.* **1938**, *60*, 499. (b) Kolthoff, I. M.; Eggertsen, F. T. *J. Am. Chem. Soc.* **1941**, *63*, 1412. (c) Kolthoff, I. M.; Bowers, R. C. *J. Am. Chem. Soc.* **1954**, *76*, 1510.

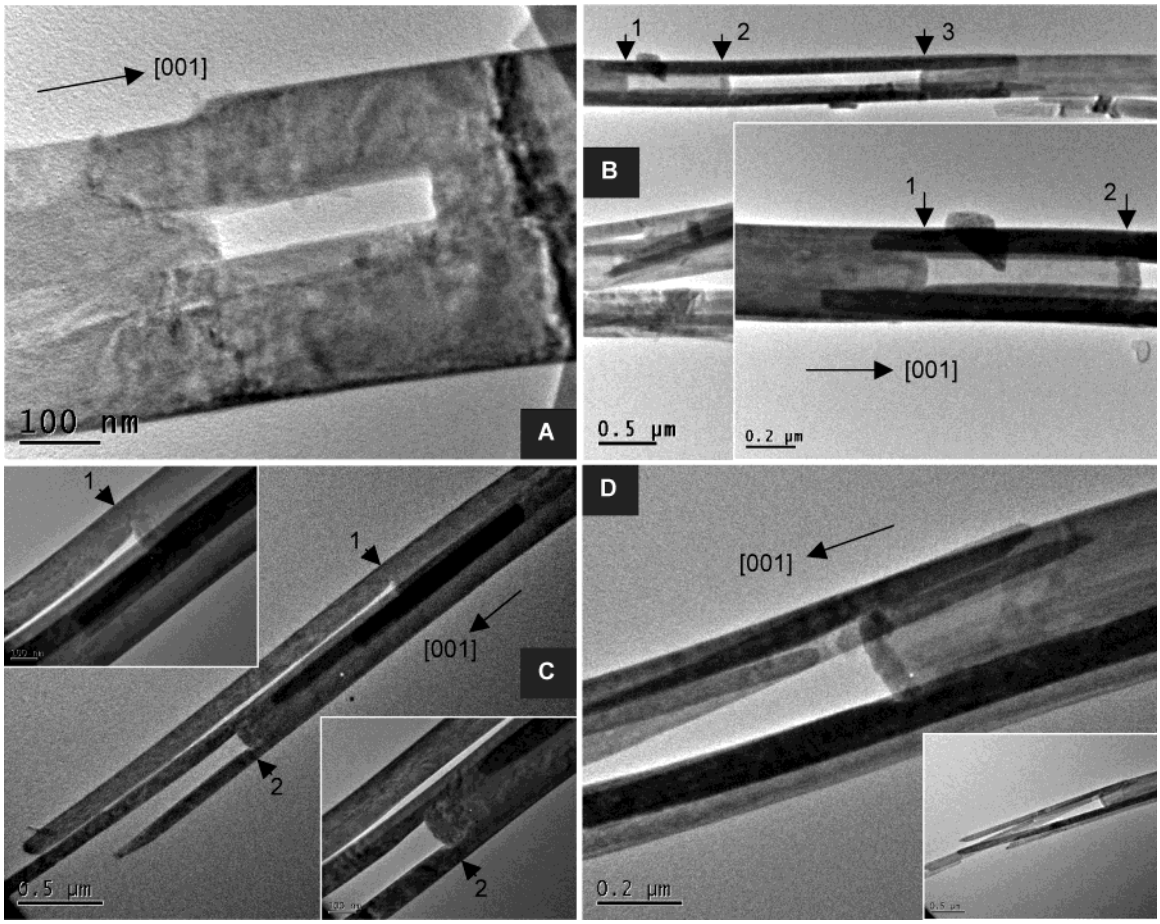

Figure 8. More complex α-MoO_3 nanostructures generated from intercrystallite connections: (A) L + R structure with inward overlapping of the secondary arms (sample from Figure 3), (B) 2L + R structure prepared with 0.033 g of TiO_2-capped α-MoO_3 nanorods, 0.050 g of $((NH_4)_2O)_{0.0866}{\cdot}MoO_3{\cdot}0.231H_2O$, and 10 mL of HNO_3 solution at 200 °C for 8 h, (C) a nano-trident formed from single-arm overlapping (sample of (B)), and (D) a nano-paintbrush formed from stacking of a forklike nanorod with smaller α-MoO_3 crystallites (sample of (B)). Numbered arrows indicate TiO_2-MoO_3 junctures in the capping areas.

nanostructures had been generated via the cementing mechanism during the hydrothermal reactions, although the effect of additional ultrasonic treatments on the attachment processes cannot be entirely ruled out at the present stage.

With prolonged ultrasonic treatments, however, the secondary α-MoO_3 arms can be detached from their main stems, producing α-MoO_3 nanorods with sizes smaller than 100 nm. As shown in Figure 9A, uniformly sized α-MoO_3 with a width smaller than 70 nm and a length longer than a few micrometers can be obtained by sonicating long forklike crystals (Figure 9B) in acetone solution. We had previously encountered great difficulties in making α-MoO_3 nanorods in the sub 0.1 μm regime;[12] the method here seems to provide a new solution to this obstacle. On the other hand, zero-, one-, two-, or three-armed α-MoO_3 nanostructures can be attained depending on the extent of sonicating (Figure 9C and D). It must be mentioned that α-MoO_3 dissolves easily in basic solutions, while it is extremely stable under acidic conditions. In this regard, the current approach is highly versatile because α-MoO_3 can be utilized as templates in making other complex-shaped nanomaterials. As had been evidenced in Figure 2D, individual square- and horseshoe-like TiO_2 nanocrystals can be obtained after removal of 1D α-MoO_3 templates in basic mediums. Integrated TiO_2 nanocrystal sheets have also been prepared with this template method (not shown). With the complex nanostructures of α-MoO_3 fabricated in this

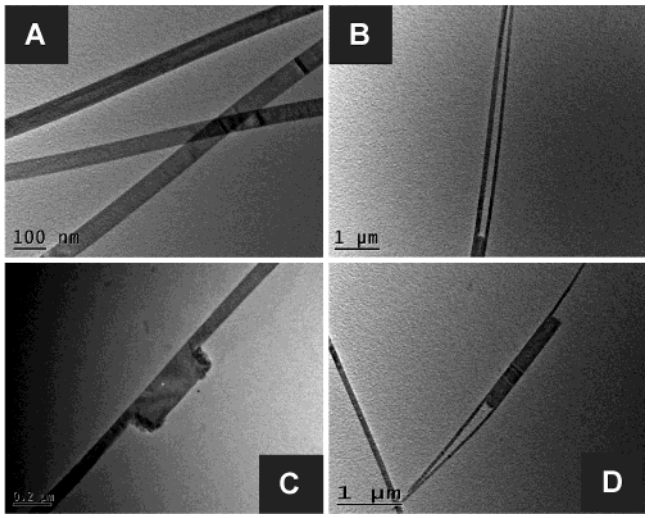

Figure 9. (A) Single-crystalline α-MoO_3 nanorods (the secondary arms of forklike α-MoO_3) resulted from prolonged sonicating in acetone for 2.5 h. (B) A long-armed α-MoO_3 nanorod. (C) A two-armed α-MoO_3 nanorod after sonication (1 h). (D) A three-armed α-MoO_3 nanorod after sonication (2.5 h).

work, more complicated TiO_2 and other nanostructures can be prepared accordingly in the future.

Regarding a further development of the present method, structural compatibility and chemical dissimilarity are two

important factors in searching for new capping and stem materials in this type of complex nanobuilding block synthesis with controlled geometry. Furthermore, a careful search for self-assembly conditions should allow us to come up with new process schemes with a higher yield and organization selectivity. Apparently, as an example here, there exist tremendous research opportunities in the synthesis and assembly of inorganic-material-capped nanostructures without the assistance of organic surfactants and ligands.

Conclusions

In summary, four-armed α-MoO_3 building blocks can be prepared with our TiO_2-capping method through manipulating growth directions at hydrothermal conditions. Because of the external bonding capacity and self-assembly of these novel nanounits, other geometrically complex α-MoO_3 nanostructures such as armed and/or holed forklike rods, tridents, and paintbrushes can also be fabricated. The present synthetic scheme is highly versatile. Under prolonged sonication, the forklike α-MoO_3 crystals can be changed into less armed nanostructures while producing smaller nanorods with widths $<$100 nm. On the other hand, the α-MoO_3 can be used as templates for making other complex nanomaterials such as anatase TiO_2 in this study. It is anticipated that the model scheme developed here can also be extended to other oxide and sulfide nanocomponents to constitute a complete nanotoolbox.

Acknowledgment. The authors gratefully acknowledge research funding cosupported by the Ministry of Education and the National Science and Technology Board, Singapore.

JA029086H